Human Molecular Genetics, 2012, Vol. 21, No. 12 **2663–2676**
doi:10.1093/hmg/dds091
Advance Access published on March 7, 2012

Genetic ablation of *Pals1* in retinal progenitor cells models the retinal pathology of Leber congenital amaurosis

Seo-Hee Cho[1,4,*], Jin Young Kim[1,4], David L. Simons[2], Ji Yun Song[1,4], Julie H. Le[1], Eric C. Swindell[1], Milan Jamrich[3], Samuel M. Wu[2] and Seonhee Kim[1,4,*]

[1]Pediatric Research Center, Department of Pediatrics, University of Texas Health Science Center, Houston TX 77030, USA, [2]Cullen Eye Institute and [3]Department of Molecular and Human Genetics, Baylor College of Medicine, Houston TX 77030, USA and [4]Shriners Hospitals Pediatric Research Center and Department of Anatomy and Cell Biology, Temple University School of Medicine, Philadelphia, PA 19140, USA

Received November 23, 2011; Revised February 9, 2012; Accepted February 29, 2012

Mutation of the polarity gene Crumbs homolog 1 (*CRB1*) is responsible for >10% of Leber congenital amaurosis (LCA) cases worldwide; LCA is characterized by early-onset degenerative retinal dystrophy. The role of *CRB1* in LCA8 pathogenesis remains elusive since *Crb1* mouse mutants, including a null allele, have failed to mimic the early-onset of LCA, most likely due to functional compensation by closely related genes encoding Crb2 and Crb3. Crb proteins form an evolutionarily conserved, apical polarity complex with the scaffolding protein associated with lin-seven 1 (Pals1), also known as MAGUK p55 subfamily member 5 (MPP5). Pals1 and Crbs are functionally inter-dependent in establishing and maintaining epithelial polarity. *Pals1* is a single gene in the mouse and human genomes; therefore, we ablated *Pals1* to establish a mouse genetic model mimicking human LCA. In our study, the deletion of *Pals1* leads to the disruption of the apical localization of Crb proteins in retinal progenitors and the adult retina, validating their mutual interaction. Remarkably, the Pals1 mutant mouse exhibits the critical features of LCA such as early visual impairment as assessed by electroretinogram, disorganization of lamination and apical junctions and retinal degeneration. Our data uncover the indispensible role of Pals1 in retinal development, likely involving the maintenance of retinal polarity and survival of retinal neurons, thus providing the basis for the pathologic mechanisms of LCA8.

INTRODUCTION

Photoreceptors in the mammalian retina initiate phototransduction, which transforms light into chemical signals that trigger the image-forming process in the retina. Rods and cones, the major vertebrate photoreceptors, are polarized cells with apical membranous extensions consisting of inner and outer segments (IS and OS), a cell body and a synaptic terminus. OS contain opsin proteins and the machinery for photo-signal transduction in stacked membrane discs. Abnormal development or formation of the OS is related to retinal degeneration (1,2). Photoreceptor cells adjoin to other photoreceptor cells or Muller glia at the top of the outer nuclear layer (ONL) by forming an adhesion belt, the outer limiting membrane [OLM (3)], which is derived from the apical junction complex (AJC) at the apical edge of the embryonic retina. The AJC and OLM collectively establish and maintain the polar structure, adhesion and integrity of the developing and mature retinal epithelia.

Leber congenital amaurosis (LCA) is characterized by severe visual impairment at birth or the first few months of life, and is thought to be caused by either abnormal development or the premature degeneration of early-stage photoreceptor cells (4). The hallmark of LCA symptoms is the absence or severe reduction of the electroretinogram (ERG). The early-onset and severity of the symptoms make LCA

*To whom correspondence should be addressed. Tel: +1 2159269361; Fax: +1 2159269325; Email: seo.hee.cho@temple.edu (S.-H.C.); seonhee.kim@temple.edu (S.K.)

distinguishable from closely related diseases such as retinitis pigmentosa (RP), which exhibits weak, late-onset retinal degeneration. Owing to its rarity, early-onset and difficulty in obtaining diseased LCA tissues, the investigation of the cellular and molecular mechanisms underlying the development of retinal degeneration has been hampered. Genetic studies have shown that mutations in several genes cause both LCA and RP, loosely depending on the nature and strength of the mutations (4). One such example is *CRB1*, which causes both LCA8 (OMIM604210) and RP12 (5–8).

Crb1 encodes a transmembrane protein that forms a tripartite evolutionarily conserved complex with Pals1 (9,10) and the Pals1-associated tight junction [Patj (11–13)], located at the epithelial tight junction (12,14–16). The Crb polarity complex and its interacting Par complex, comprised of Par3, Par6 and atypical protein kinase C (aPKC), play an important role in polarity determination, maintenance of apico-basal polarity and establishment of cell–cell junctions (17–19). Unlike human patients, mouse *Crb1* mutants, including the knock-out (KO) mouse, show only characteristics of RP (RP12) such as late-onset, focally disorganized retinal phenotypes due to adhesion defects between the photoreceptors and Muller glia cells at the OLM in the adult retina (6,14,20,21). Although *Crb2* does not contribute to human RP or LCA (22), the lack of a severe early-onset LCA phenotype in *Crb1* KO mice may result from a functional compensation by its homologs Crb2 and 3. We hypothesized that since *Pals1* is a single gene in mice and humans, is an essential component of the Crb polarity complex (23) and is required for Crb1 localization in the subapical region of the Muller glia (14), conditional ablation of the *Pals1* gene in the developing retinal progenitor cells would block the assembly of the functional Crb polarity complex. Our study shows that a *Pals1* deletion causes the death of newly born retinal neurons, adhesion defects, disrupted apical structure and photoreceptor degeneration, which lead to early visual impairment, mimicking the human LCA phenotypes.

RESULTS

Crb polarity complex genes are expressed in retinal progenitor cells

As the extremely early manifestation of *CRB1*-mediated LCA8 symptoms in human patients indicates, it is likely that the Crb polarity complex proteins are essential in establishing and maintaining apico-basal polarity of the retinal progenitor cells during embryonic development. Thus, we first analyzed the expression and distribution of the *Crb* polarity complex genes and proteins in developing retinas, using immunofluorescence. For this assay, we used three antibodies specific to Pals1, Patj and pan-Crb (Crb1, 2 and 3). As expected, all three core Crb polarity complex proteins (Crbs, Pals1 and Patj) were localized along the apical edge of the retina at all of the embryonic stages analyzed (Fig. 1A–C). This localization pattern demarks the AJC, a primitive structure of the OLM of the adult retina where junctional proteins are located (Fig. 1D and D′). In the embryonic AJC, Crb proteins localize apically to the AJ proteins, N-cadherin and β-catenin (see insets), which may correspond to sub-apical region of photoreceptor cells. AJC localization of the Crb complex proteins was maintained in the OLM of the adult retina. Unlike the apical localization of proteins, *Pals1* transcripts were distributed in the entire developing retinas at E12.5 and E14.5, though weakly expressed (Fig. 1E and F). At E14.5, *Pals1* expression was more enriched in the progenitors in the outer neuroblastic layer than in those of early-born neurons in the inner neuroblastic layer. We found that *Pals1* distribution in the proliferating zone in the outer neuroblastic layer was similar to that in the ventricular zone of the cerebral cortex (24), which was consistent with results from a previous *Crb1* expression study in the developing retina (25).

Pals1-deficiency-mediated polarity ablation induces microphthalmia and retinal lamination defects

To study the function of Pals1 during retinal development and to generate a new LCA8-like model, we conditionally ablated the *Pals1* gene in the developing retina using standard Cre-loxp technology. Selectively deleting *Pals1* gene function in retinal progenitor cells circumvents the early lethality in the *Pals1* KO embryos, which show gastrulation defects and die at or around E8.5 and E9.5, in which eye organogenesis is not initiated (data not shown). To ablate the *Pals1* gene in the retina, we used Rx-Cre (26), in which Cre was previously shown to be enriched in the retinal progenitor cells from the beginning of eye development, hence making this Cre line ideal for the selective ablation of *Pals1* in the entire retinal progenitor cell population, as well as in their descending retinal neurons. When we examined the Cre expression pattern using the ROSA26R-lacZ indicator line, the Rx-Cre line showed a somewhat variable degree of Cre expression in retinal progenitor cells at E15.5 (Fig. 1G–I) and in the mature *Pals1*-deleted retina at P35 (Fig. 1J and K). In addition, other neighboring non-neural tissues like the ciliary body, iris, retinal pigmented epithelium (RPE), lens and forebrain showed varying degrees of Cre expression. We also used another retina-specific Cre transgenic line, Chx10-Cre, but the resulting phenotypes were weaker, potentially due to a delayed and heterogeneous Cre expression in retinal progenitor cells (27).

Pals1 conditional knock-out (CKO) mice (*Pals1*$^{flox/flox}$; *Rx-Cre*) showed no obvious external defects other than the occasional moderate-to-severe microphthalmia (Fig. 1L–N). We then examined embryonic and postnatal retinas for defects in retinal lamination, common phenotypes observed in retinas with polarity defects (28–30). Locally disorganized regions were occasionally detected in *Pals1*-deficient retinas emerging at E15.5. In addition, lamination defects such as retinal folds became more frequent and prominent at E17.5 compared with those of wild-type (WT) controls (Fig. 2A, B, F and G). *Pals1*-deleted embryonic retinas showed variable thickness compared with the WT littermates, due to retinal folding (Fig. 2B and G). At P0, localized pseudorosettes were formed more regularly and displayed a mature shape, and thinning and disorganization of the inner plexiform layer and ganglion cell layer became evident (Fig. 2C and H). At P14 and onward, the retinal laminar was fully developed in WT mice, whereas the lamina of the Pals1-deficinet retinas became locally thinner and

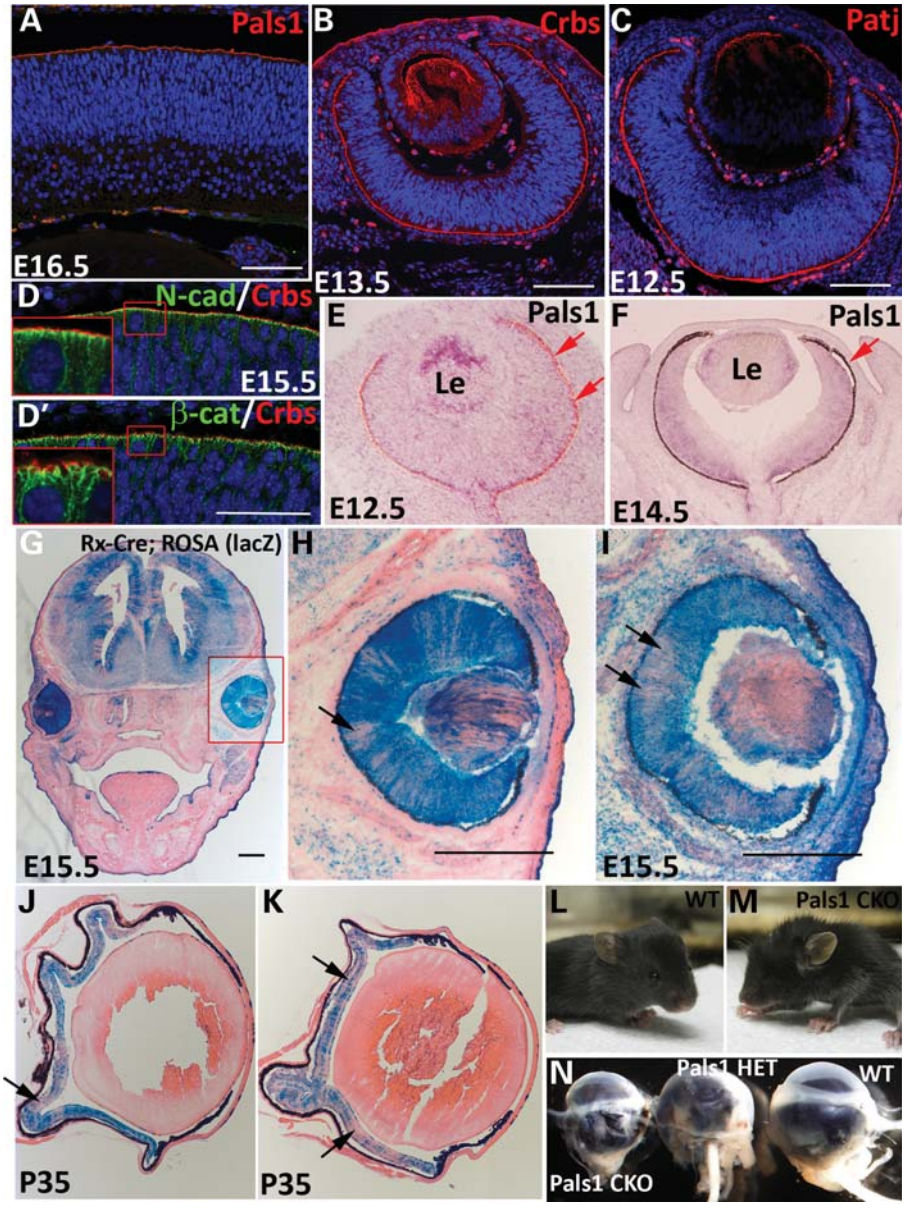

Figure 1. Expression and localization of Crb polarity complex proteins at the apical margin of the retinal epithelia. Immunostaining of Pals1 (**A**), pan-Crb (**B**) and Patj (**C**) proteins in WT retinas at E16.5 (A), E13.5 (B) and E12.5 (C). (**D** and **D′**) AJC localization of Crb proteins shown with adherens junction markers, N-cadherin (upper) and β-catenin (lower) at the apical margin of E15.5 retinas. Note that the enlarged images (insets) show apical localization of Crb proteins relative to AJ proteins in the AJC. (**E** and **F**) *Pals1 in situ* hybridization at E12.5 and E14.5 shows weakly expressed transcripts in retinal epithelia. Red arrows demark the RPE. (**G**–**K**) Determination of Cre expression in ROSA26R-lacZ;Rx-Cre mice by X-Gal staining followed by eosin counterstaining. Two representative X-gal-stained images show the non-homogeneous Cre expression in developing WT retinas at E15.5 (arrows in H and I) and adult *Pals1* CKO retinas at P35 (arrows in J and K). (**L** and **M**) Representative images of WT (L) and *Pals1* CKO (M) mice at P23 show an infrequent microphthalmia phenotype in *Pals1* CKO. (**N**) Eyeballs harvested from 5-month-old *Pals1* CKO, heterozygote and WT littermates for size comparison (left to right). Le, Lens. Scale bars (A–D), 48 μm; (G–I), 200 μm.

severely disorganized (Fig. 2D, E, I and J). Pseudorosette formation is reminiscent of a *Crb1* KO phenotype, in which the defect in cellular adhesion between the photoreceptors and Muller glia cells caused focal rosette formation in the adult stages (31). In addition, we observed a shortening (or complete absence) of the IS and OS of photoreceptor cells at P14 and P60 compared with those in the WT control retinas (Fig. 2D1, E1, I and J). At the adult stages, such as P60 and P35, the *Pals1* CKO retinas are generally devoid of the photoreceptor layer, either partially or completely (Fig. 2E and E1, and data not shown). Furthermore, we observed the degeneration of other retinal cells in the inner nuclear and ganglion cell layers during the early postnatal stages, which progressively worsened at later stages (data not shown). As a result, the ONL was completely absent in the severely affected adult retinas (Fig. 2E), whereas the inner nuclear and ganglion cell layers were less severely affected. However, we noticed some degree of phenotypic variation among *Pals1* CKO retinas at all of the examined stages.

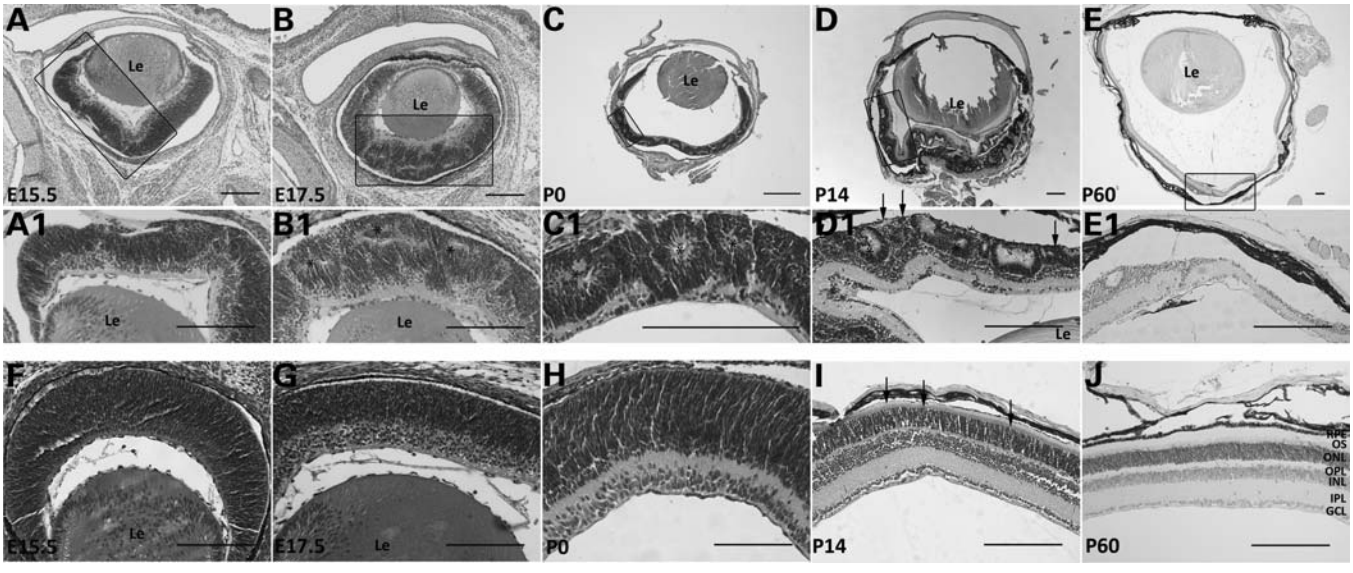

Figure 2. Progressive lamination defects and degeneration of *Pals1* CKO retinas. H&E staining of retinas from WT control (bottom row) and *Pals1* CKO mice (top two rows) at E15.5 (**A**, **A1** and **F**), E17.5 (**B**, **B1** and **G**), P0 (**C**, **C1** and **H**), P14 (**D**, **D1** and **I**) and P60 (**E**, **E1** and **J**) reveals the defects in retinal lamination, IS and OS formation and survival of the photoreceptor cells. Retinal folds and/or pseudorosettes (asterisks in B1, C1 and D1), shortened or deleted IS and OS (arrows in D1) and retinal thinning (E1) are shown. Le, Lens. Scale bars, 200 μm.

Heterogeneous Cre expression in Rx-Cre may be responsible for these phenotypic variations. The retinas lacking only one copy of the *Pals1* gene (heterozygote) also showed phenotypes such as lamination defects, and pseudorosette formation, although the degree was weaker than that of the CKO (data not shown). This finding suggests a dose-dependent requirement of Pals1 function in retinal progenitor cells as observed in developing cerebral cortex (24). In addition, these results suggest that Pals1 function is essential for laminar formation in both embryonic and postnatal retinas. This represents the first finding that LCA8-like pathology can be initiated by polarity defects in retinal progenitor cells during embryonic eye development.

Pals1 loss disrupts Crb polarity complex at the apical junction of the retina

Pals1 functions as a core scaffold of the Crb polarity complex, recruiting two other proteins, Crb and Patj. In the retina, the Crb complex localizes to the AJC in the embryonic retina and the OLM of the mature retina; correct Crb localization depends on Pals1 (14). In general, the three core Crb polarity complex proteins are mutually dependent for normal localization and function.

To assess the distribution and localization of the Crb polarity complex proteins in the absence of Pals1, we performed immunostaining at P0 and P60, using Pals1- and Patj-specific and pan-Crb antibodies. The distribution of all three Crb polarity complex proteins, Pals1, Crbs and Patj, was partially disrupted or mislocalized in retinal regions with lamination defects at P0 (Fig. 3A, C, E and G, and data not shown). Compared with Ezrin staining, which localizes to the apical villi of the surrounding the RPE that lies immediately apical to AJC, Pals1 or pan-Crb staining in *Pals1* CKO retinas was abnormally detected in the inner retinas, unlike in the WT counterpart, in which they localize at the AJC. This ectopic localization marks the apical edge in the inner surface of the premature pseudorosettes (or retinal folds), where IS and OS are located. In addition, the discontinuation and disruption of Pals1 and Crb-1 localization at the AJC were seen in the apical edges of the P0 *Pals1* CKO retinas (Fig. 3E and G). At P60, the apical localization of the Crb complex proteins, Pals1 and Crbs, in the OLM was frequently absent or diffused (Fig. 3B, D, F and H). Furthermore, the apical distribution of Par3, a core member of the Par polarity complex containing Par3/Par6/aPKC, was disturbed in the *Pals1*-deficent retinas (Fig. 3I and J), supporting the previously described interaction between two collaborative apical polarity complexes (17,18). In addition, we determined the integrity of the adherens junctions by β-catenin immunostaining, which revealed a disorganization of adherens junctions as shown by the lack of β-catenin localization at the apical surface of the *Pals1* CKO retina at P60 (Fig. 3K and L). We also examined the apical extensions of the photoreceptor cells, IS and OS (Fig. 3D and H). The gap between the OLM (red Crb staining) and apical villi of the RPE cells (green Ezrin staining) normally contains the OS and part of the IS of the photoreceptor cells. In *Pals1*-deleted retinas, the complete absence or apparent shortening of these structures was clearly demonstrated. Together, these results support the notion that the scaffolding function of Pals1 is required for the proper assembly and maintenance of the apical polarity complex proteins and the apical structures in the retinal epithelia and photoreceptor cells.

We further investigated the cellular defects of photoreceptor cells in *Pals1* CKO retinas, using transmission electron microscopy at P21, when the retinal lamination is in the process of deterioration. We observed that the *Pals1*-deficient ONL generally exhibits a thinner and less regular appearance. Oftentimes, the ONL was locally extruded outward to the RPE side and some photoreceptors lacked both IS and OS

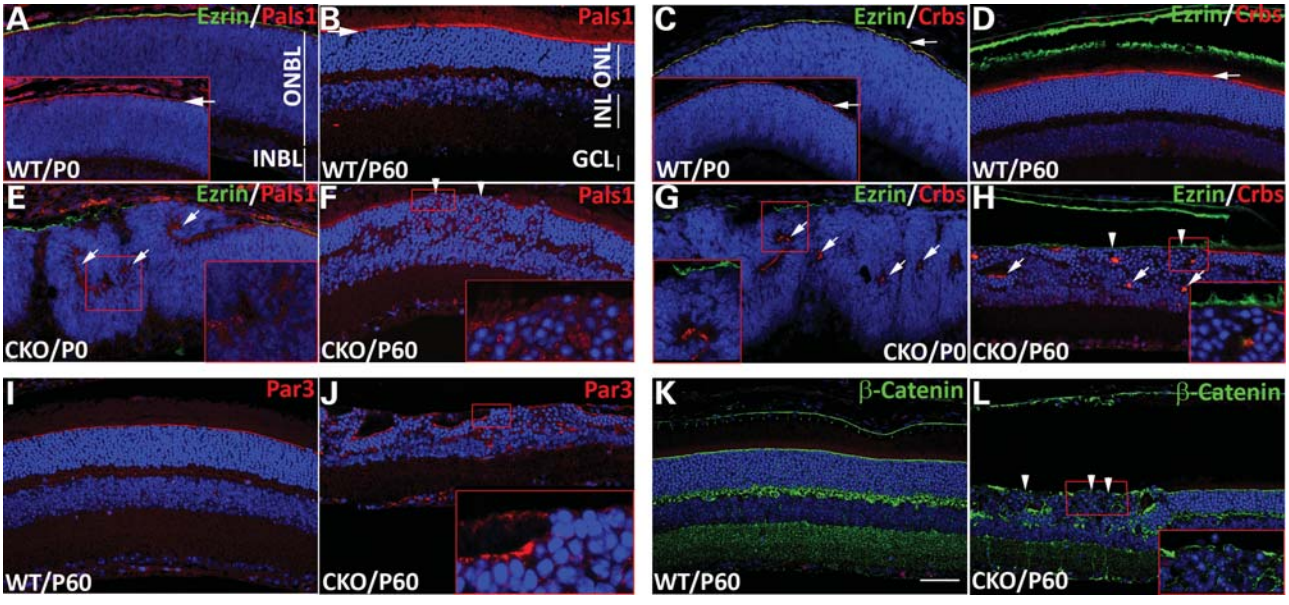

Figure 3. Disruption of apical polarity complex proteins and apical junction by *Pals1* ablation. Immunostaining of Pals1 (red in **A**, **B**, **E** and **F**) and Crbs (red in **C**, **D**, **G** and **H**) on WT (A–D) and *Pals1* CKO retinal sections (E–H) at P0 (A, C, E and G) and P60 (B, D, F, and H) shows disruption and internalization of apical Pal1 and Crbs staining in retinal epithelia. Insets in (A) and (C) show Pals1 and Crbs, respectively, staining (white arrows) at the AJC. Ezrin staining (green in A, C, D, E, G and H) marks the apical process (or villi) of RPE cells, which lies on top of the AJC. Arrows in (E), (G) and (H) indicate mislocalized Crb complex proteins in the middle of retinal epithelia, and arrowheads in (F) and (H) indicate the absence of Pals1 and Crbs in the OLM of the adult retinas, respectively. (**I**–**L**) Localization of Par3 (red in I and J) and β-catenin (green in K and L) at the OLM of the retina is also disrupted in *Pals1* CKO retinas (J and L) compared with WT control (I and K) at P60 (arrowheads). Scale bar, 48 μm.

(Fig. 4A–D). Pseudorosettes formed by the abnormal aggregation of rods contained short and distorted OS and IS (Fig. 4B, inset), which is consistent with remaining R4D2 staining in the inner lumen of the pseudorosettes (Fig. 6B). As a result, photoreceptor cell bodies in the ONL were juxtaposed to the RPE, consistent with the previous findings [Fig. 4B and C, 2D, 6A and B (2)]. Similar to the adherens junction defects reported previously in *Crb1*$^{-/-}$ mouse (21), apical junctions (OLM) were disrupted in the area of disorganized lamina (Fig. 4D). Junctions were relatively intact where the OLM is maintained, although the OS were shorter (Fig. 4C). In addition, the OLM was discontinuous and disrupted in the retinal regions exhibiting ONL laminar defects, supporting the notion that the laminar defects in *Pals1* CKO retinas resulted in part from defects in apical junction formation in the OLM (Fig. 4C and D). When the OS of photoreceptor cells are preserved, they are often significantly reduced in size and exhibit a rounded rather than elongated morphology (Fig. 4E and F). Pycnotic cells were also found occasionally in the ONL, confirming the observation of cleaved caspase 3^{+} (CC3^{+}) cells in *Pals1* CKO adult retinas (Figs 4C and D and 7O). These results suggest that polarity complex proteins, including Pals1, are essential for forming specialized apical substructures, OLM, IS and OS, to maintain apical polarity of the retina and adhesion among retinal cells.

Pals1-deficient mice are visually impaired

Histologic and transmission electron microscopy analyses of the *Pals1*-deleted retinas shown in Figures 2 and 4 revealed not only retinal lamination defects and hypocellularity but also a reduction in thickness of IS and OS occurring throughout postnatal development. Although variations of the severity exist among genotyped animals, *Pals1* CKO retinas at P60 can be generally characterized by the thinning or disorganization of the ONL (Fig. 5F–M). Remarkably, some of the *Pals1*-deficient retinas preserve the majority of the photoreceptor cells at P60 (Fig. 5G and H), which likely resulted from the heterogeneity of the Cre expression in our Rx-Cre transgenic line. Since previous work implicated abnormal development of the OS of photoreceptor cells in retinal degeneration, we anticipated that these *Pals1*-deficent retinas possess limited visual capacity (1,2,32).

To determine the visual activity of *Pals1* CKO animals, we applied scotopic ERG, measuring the electric response of the retina after dark adaptation. WT retina at P60 showed increased electrical responses of photoreceptor cells (a-wave) and interneurons (b-wave) as the intensity of the flash light increased (Fig. 5A). However, both a- and b-waves were reduced or almost undetectable in *Pals1*-deficient retinas ($n = 4$), suggesting severe defects in visual function in *Pals1* CKO mice (Fig. 5B–D). When we plotted the b-wave response, we found that most of the *Pals1* CKO mice showed a decreased ERG response except in one *Pals1* CKO retina that showed a less compromised visual function and undisturbed retinal morphology (CKO22L in Fig. 5E, and data not shown). We observed a close correlation between the retinal histologic phenotypes and ERG responses. The *Pals1* CKO mouse with severe retinal morphologic defects shows the most severely affected ERG response. This observation agrees with a previous finding that OS dysplasia has a strong correlation with ERG loss in the *Rp1* CKO mouse (33). In addition, we determined

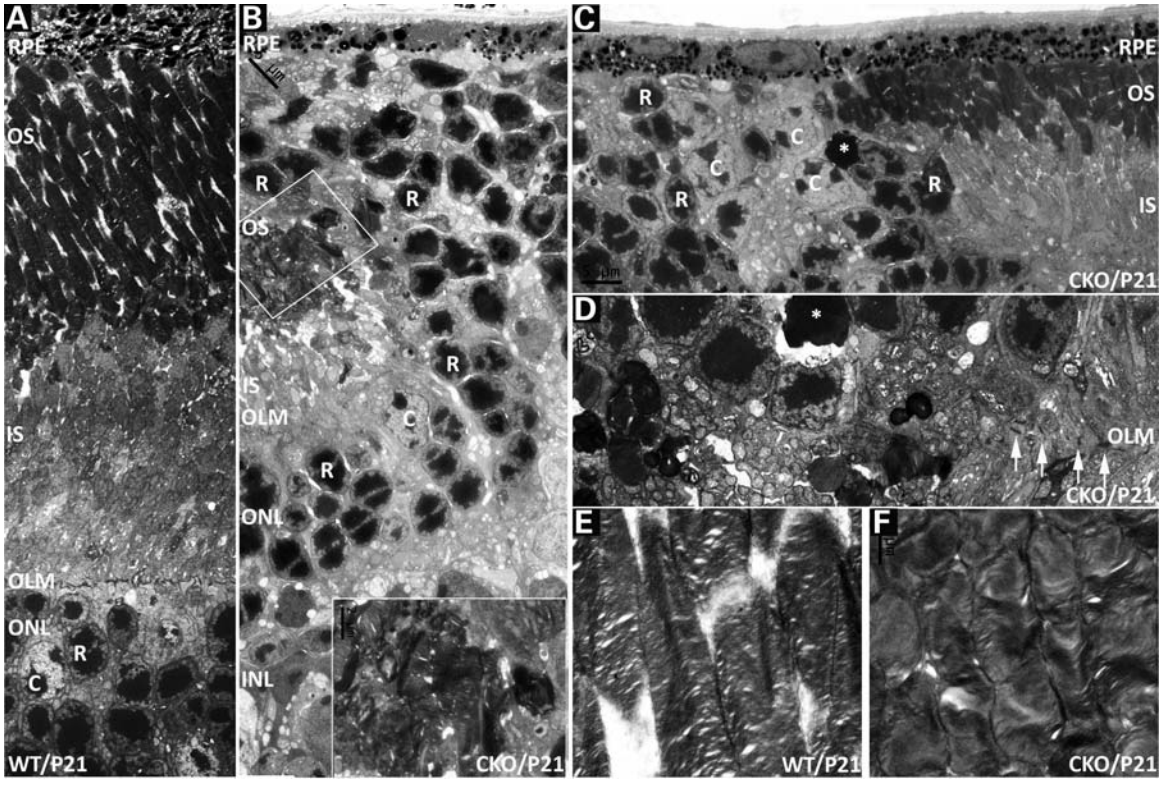

Figure 4. Subcellular phenotypes of *Pals1*-deficient retinas. Electron microscopic analysis at P21 reveals defects in the OLM, IS and OS. (**A**) WT retinal region corresponding to parts of the ONL, OLM, IS and OS is shown. OLM is located at the top of the ONL containing photoreceptor cells, rods and cones. (R, rod; C, cones). (**B**) *Pals1* CKO retina shows apical protrusion of the ONL, the inner nuclear layer's intrusion to the ONL and the disrupted IS and OS remaining within the pseudorosette (inset). As a result, photoreceptor cells are juxtaposed with the RPE while OS are in direct contact with the overlying RPE. (**C**) The gradual shortening and deletion of IS and OS and abnormal arrangement of photoreceptor cells become evident at the border between affected and unaffected areas. Apoptotic cells in (C) and (D) are marked with an asterisk. (**D**) Discontinuation of the OLM is demonstrated by the absence of the arrows in *Pals1*-deficient retinas. (**E** and **F**) The OS are shorter and disorganized in *Pals1* CKO retinas compared with the elongated morphology in WT (E). Scale bars, 1 to 5 μm.

the retinal activity of younger animals to determine the initial stage at which *Pals1* CKO mice begin to lose vision. When *Pals1* CKO mice were subjected to ERG at P21 ($n = 2$) and P35 ($n = 4$), we observed a severely reduced ERG response in some of the CKO mice when compared with WT littermates (data not shown). Although we further attempted to determine ERG responses in P14 *Pals1* CKO mice, which had just opened their eyes, we were unable to measure a reliable ERG recording because of the reduced size of the eye opening in these mice. Based on this result, we suspect that both photoreceptor and non-photoreceptor cells show defects in visual responses, and degeneration of the retinal photoreceptor cells is not a prerequisite of the vision loss in LCA patients. Rather, the subcellular defects in the photoreceptor cells, such as OS shortening and irregular lamination, can impair normal visual function in *Pals1* CKO mice.

Abnormal retinal cells in *Pals1*-deficient retinas

Polarity complex proteins are not only important for establishing apico-basal polarity in epithelial cells, but are also involved in many critical cellular processes such as fate determination, directed cellular migration and development of specialized cellular structures (24,34). Of these processes, cell fate determination involving asymmetric inheritance of fate determinants in daughter cells is exemplified in *Drosophila* neuroblasts (35,36). In the developing cerebral cortex, the deletion of *Pals1* induces precocious differentiation of cortical progenitor cells, leading to the depletion of the progenitor pool (24).

To examine the effects of *Pals1* CKO-mediated polarity disruption on retinal neurogenesis and survival, we examined the presence and distribution of retinal neurons at two postnatal stages. Since primary retinal differentiation and lamination are completed by P14, analysis at this stage provides a window in which to examine the completion of retinal neurogenesis. Additionally, we choose P60 to study the survival of seven different retinal cells, using retinal cell-type-specific markers. At P14, when *Pasl1* CKO retinas undergo localized lamination defects manifested by retinal folds or pseudorosette formation, all of the retinal markers were present but most were reduced in number and misplaced, whereas retinal thinning and hypocellularity were evident at P60. For example, the photoreceptor OS-specific R4D2 staining partially disappeared at the retinal apical margin, and was subsequently concentrated in the photoreceptor cell body in the defective region (Fig. 6A and B). Apical cone cells marked by cone arrestin immunostaining at IS, OS and synaptic termini were also reduced in number, and cone segments were shorter and deformed. At P60, the OS-specific R4D2 stain was almost

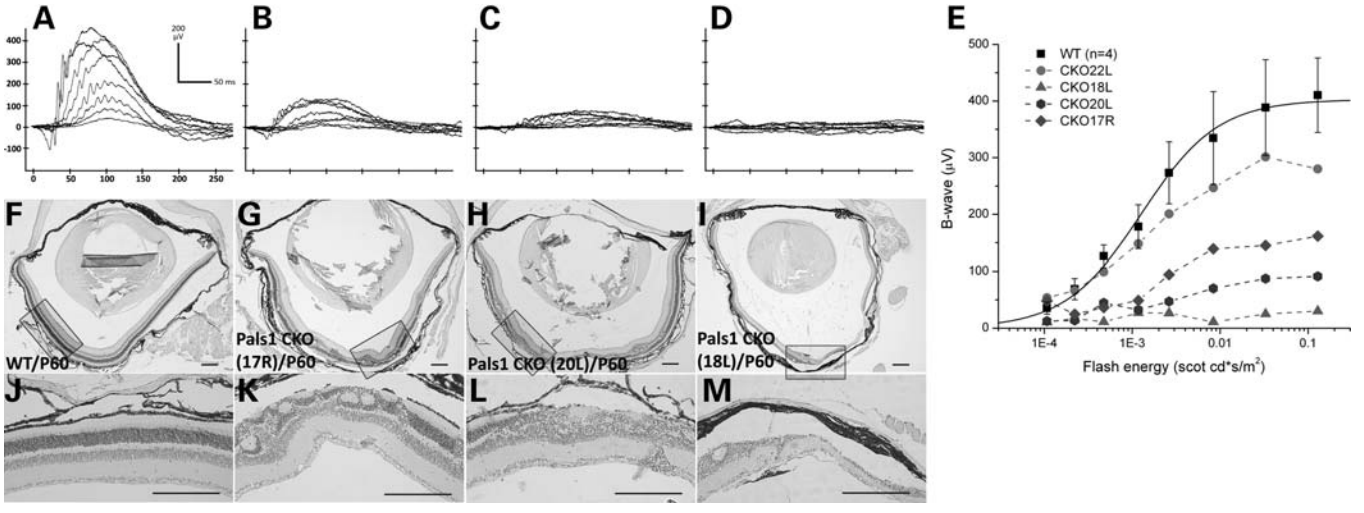

Figure 5. Impaired visual response of *Pals1*-deficient retinas. Raw ERG waveforms of WT (**A**) and three *Pals1* CKO retinas (**B**–**D**) at P60. Scotopic b-wave was recorded from P60 WT and *Pals1* CKO mice to a series of flash lights ranging in intensity from −3.81 to −0.79 log scotopic cd/m^2. (**E**) Plots of the maximum b-wave amplitudes for increasing intensity of flashing light for WT (square) and *Pals1* CKO mice. Note that four different *Pals1* CKO retinas show heterogeneous ERG responses. (**F**–**M**) Matched H&E staining shows different degrees of the global morphologic defects, ranging from disorganized lamination, photoreceptor segment shortening/deletion and degeneration. (J–M) Close-up images of WT and *Pals1* CKO retinas are shown. Scale bars, 200 μm.

completely absent though its cytoplasmic accumulation remained relatively unchanged (Fig. 6C and D). Cone cells expressing cone arrestin were clearly decreased and morphologically abnormal at P60. Overall, the total photoreceptor cell number was greatly reduced at P60 (Fig. 6C and D). Pax6$^+$ amacrine and ganglion cells were relatively normally distributed at P14 and P60, although some apically misplaced Pax6$^+$ cells indicated a severe retinal tissue polarity defect in *Pals1* CKO (Fig. 6E–H). Total Pax6$^+$ cells were greatly reduced at both stages. GS staining at the apical processes of the Muller glial cells was locally absent at the OLM of the *Pals1* CKO retinas at P14 and P60, showing that the apical junctions (OLM) formed between Muller glia and photoreceptors are defective (Fig. 6E–H). Bipolar and horizontal cells stained with Chx10 and calbindin antibodies, respectively, were reduced in number, but relatively normally localized with the exception of some bipolar cells ectopically located in the apical region of the *Pals1* CKO retinas at P14 (Fig. 6I and J). The neuronal marker, β-tubulin, was also ectopically distributed at the apical region of *Pals1* CKO retinas, and the thickness of the inner plexiform layer was significantly decreased at both stages (Fig. 6M–P).

In summary, *Pals1* CKO retinas show multiple phenotypes, including OS dysplasia, degeneration and mislocalization of retinal neurons, suggesting essential roles for Pals1 in forming the apical structure of the photoreceptor cells, maintaining the laminar organization and supporting the survival of the retinal cells.

Cell proliferation was variably affected in *Pals1*-deficient retinas

As the previous histologic and marker analyses suggested the loss of retinal cells in *Pals1* CKO retinas, we next explored whether polarity disruption exerts any effects on the self-renewal and maintenance of the retinal progenitor cells.

We used BrdU, a thymidine analog, to determine the size of the pool of retinal progenitor cells undergoing the S-phase of cell division. BrdU was injected into E15.5 and E17.5 timed-pregnant females 30 min before the tissue harvest, and mitotic retinal cells in the S- and G2-phases of the cell cycle were marked with the immunofluorescence staining using anti-BrdU antibody. In WT embryos, the retinal progenitor cells in the S- and G2-phases were positioned in the lower side of the outer neuroblastic layer (Fig. 7A). Cells in the apical side of the retina and inner neuroblastic layer lacked BrdU because M-phase cells and post-mitotic cells are located in the apical margin of the outer neuroblastic layer and inner neuroblastic layers, respectively. An apically localizing subset of M-phase cells was simultaneously determined using pH3 antibody. In *Pals1* CKO retinas, the pattern of BrdU-labeled dividing cells was disorganized in lamination-defective regions (Fig. 7B and C). As a result, the boundary between dividing (outer neuroblastic layer) and differentiated (inner neuroblastic layer) cells was not clearly defined in *Pals1* CKO retinas, and the pH3$^+$ cells were not exclusively localized in the apical side of the retina. This aberrant localization of pH3$^+$ cells in the inner retina clearly demonstrated the disruption of retinal polarity. We then quantified the fraction of BrdU$^+$ and pH3$^+$ cells from both WT and *Pals1* CKO mice. As shown in Figure 7D, the average percentage of BrdU$^+$ cells was slightly higher in *Pals1* CKO retinas at E15.5 than in WT [33.96 and 31.95%, respectively ($n = 4$ and $n = 5$)]. However, the average percentage of BrdU$^+$ cells at E17.5 was slightly reduced in *Pals1* CKO retinas (30.43 versus 28.60%, $n = 3$), suggesting potential detrimental effects on the maintenance of the progenitor pool in polarity-defected retinas. It is notable that *Pals1*-deficient retinas showed a greater extent of variation in the fraction of retinal progenitor cells undergoing cell division at E15.5 (Fig. 7D). *Pals1* CKO retinas showing the lowest and highest BrdU fractions were 25 and 39%, respectively. Quantization with pH3 staining also showed similar results (2.23% in WT versus 2.39% in *Pals1*

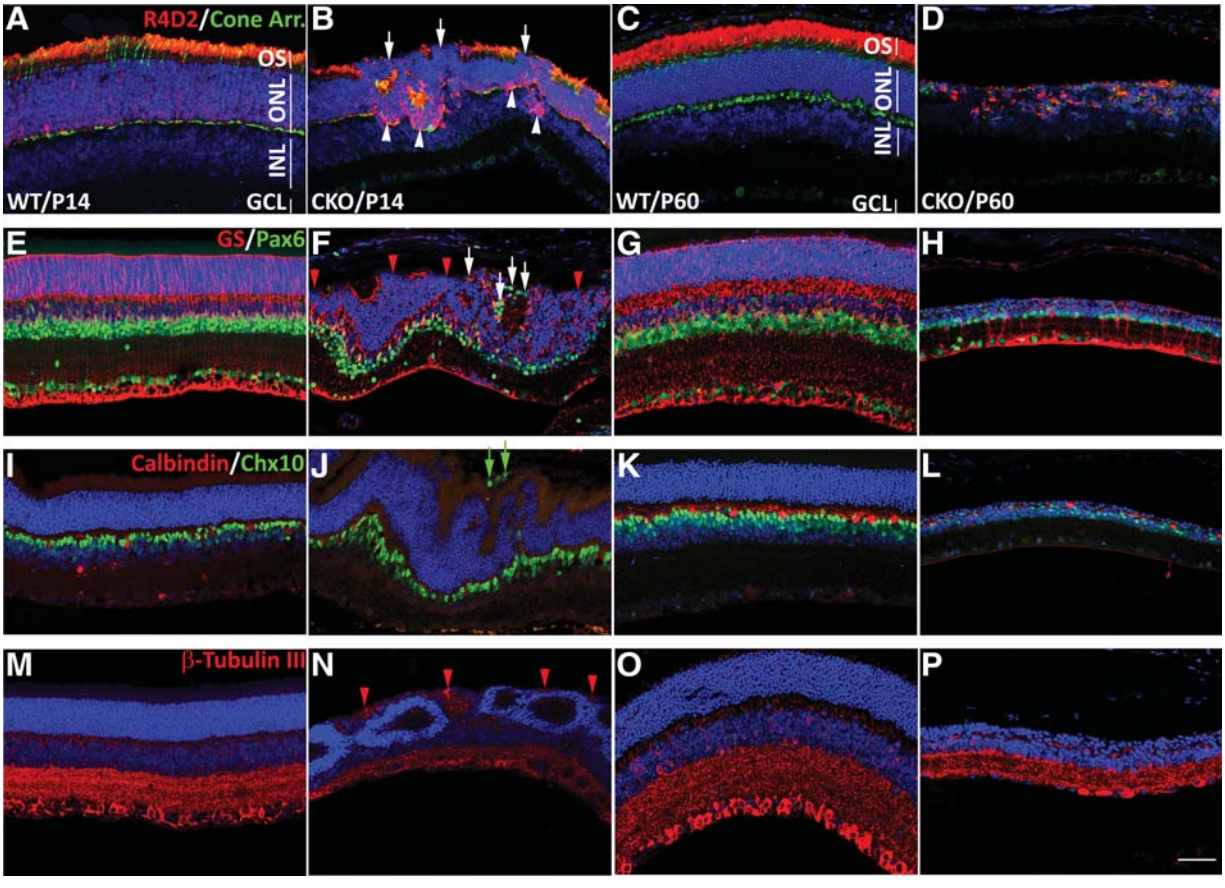

Figure 6. The effect of polarity defects on retinal neurons. Representative images of fluorescent antibody staining show the defects in expression and localization of retinal markers. WT (**A**, **C**, **E**, **G**, **I**, **K**, **M** and **O**) and *Pasl1* CKO (**B**, **D**, **F**, **H**, **J**, **L**, **N** and **P**) retinas at P14 (A, B, E, F, I, J, M and N) and P60 (C, D, G, H, K, L, O and P). (A–D) Retinal sections were stained with R4D2 (red) and cone arrestin antibodies (green). The absence and/or reduction of R4D2 staining in the OS of the photoreceptor cells (white arrows) and ectopic accumulation in the cell body (white arrowheads) around the retinal folds/pseudorosettes are demonstrated. Note that R4D2$^+$ OS are nearly completely missing at P60, whereas rod and cone cell numbers were significantly decreased. (E–H) Retinal sections were stained with Muller glia-specific GS (red) and Pax6 (green) for amacrine, ganglion and horizontal cells. The disrupted apical processes of the Muller glia cells at P14 (red arrowheads) became evident in the retinas undergoing lamination defects. Apically mislocalized Pax6$^+$ cells are marked with white arrows. (I–L) Retinal horizontal and bipolar cells were stained with calbindin (red) and Chx10 (green). Misplaced bipolar cells are shown at the apical region of *Pals1* CKO retina (green arrows). (M–P) Retinal neurons were stained with β-tubulin III (red). β-Tubulin III$^+$ processes of the retinal neurons (ganglion and amacrine cells) are apically routed (red arrowheads) and the thickness of the inner plexiform layer is reduced in *Pals1* CKO retinal sections. All retinal nuclei were counterstained with Hoechst 33342 (blue). Retinal layers are indicated with white lines (A and C); OS, outer segments; ONL, outer nuclear layer; INL, inner nuclear layer; GCL, ganglion cell layer. Scale bar, 48 μm.

CKO at E15.5 and 3.06% in WT versus 2.00% in *Pals1* CKO at E17.5), supporting the idea that *Pals1* CKO retinas might be defective in maintaining a progenitor pool. This observation in the retina contrasts with previous results showing that the pool of BrdU and pH3$^+$ cells was markedly reduced in the *Pals1*-deficient cortex (24).

Apoptotic cell death was moderately increased in *Pals1*-deficient retinas

To determine whether *Pals1*-ablated disruption of the Crb polarity complex affected the survival of retinal progenitor cells, we stained retinal sections of WT and *Pals1* CKO mice with an anti-CC3 antibody. In WT retinas at E15.5, E17.5 and P0, we observed that a low number of cells were undergoing apoptosis (Fig. 7E–G). A moderate increase of CC3$^+$ cells was observed in *Pals1*-deficient retinas throughout embryonic, early postnatal and adult stages (Fig. 7H–J and O). Although we frequently observed dying cells in retinal regions showing lamination defects, we also observed, although less frequently, pyknotic cells in the *Pals1* CKO retinas that displayed no obvious lamination defects (data not shown). This finding suggests that cell death precedes retinal disorganization in *Pals1*-deficient mice. At E17.5, ∼76% of the dying cells were located within the INBL. We then determined the identity of CC3$^+$ cells by double-staining with antibodies against CC3, and other markers such as BrdU/cyclin D1 and Pax6, which specifically stain retinal progenitor cells and ganglion/amacrine cells, respectively. As shown in Figure 7K–M″, the majority of CC3 cells are BrdU$^-$ and cyclin D1$^-$, but are Pax6$^+$ in the *Pals1* CKO retinas, suggesting that these are newly generated post-mitotic neurons, such as ganglion and amacrine cells. This observation also indicates that *Pals1*-ablated retinal progenitors are resistant to apoptotic cell death. This is consistent with a

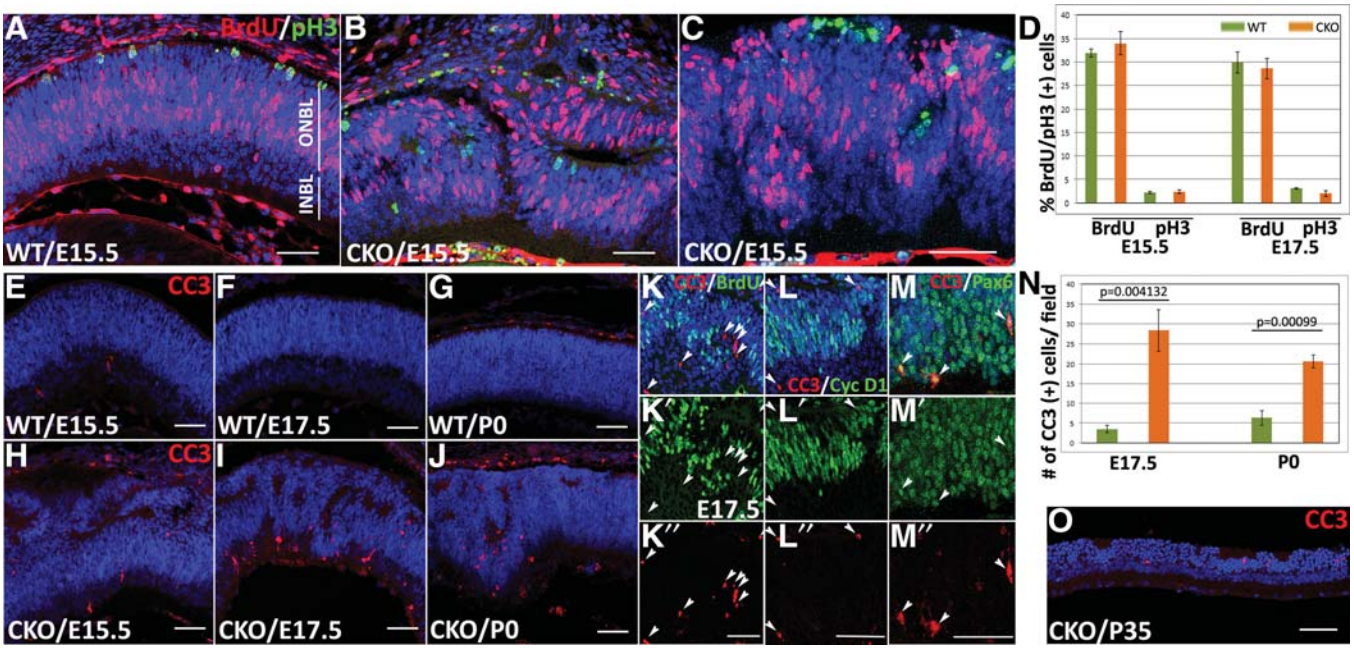

Figure 7. Altered cell proliferation and increased cell death in the *Pals1*-deficient retina. (**A**–**C**) BrdU purse labeling analysis shows normal cell proliferation behavior in the *Pals1*-deficient retina. Representative images showing the lowest and highest fractions of $BrdU^+$ cells in *Pals1* CKO retinas (B and C, respectively) are compared with that of WT (A). (**D**) Quantification of cells undergoing cell division using BrdU and pH3 immunostaining shows minor differences at both E15.5 and E17.5 in both WT and *Pals1*-deficient retinas. (**E**–**J**) Increased number of apoptotic cells were detected in embryonic and neonatal *Pals1* CKO retinas. Anti-CC3 staining (red) at E15.5 (E and H), E17.5 (F and I), P0 (G and J) and P35 (**O**) show increased number of apoptotic cells in *Pals1* CKO (H–J) compared with WT (E–G). (**K**–**M**) Double-staining with CC3 (red) and other progenitor/early neural markers (green) shows that the majority of $CC3^+$ cells are $BrdU^-$ and cyclin $D1^-$, but $Pax6^+$ at E17.5 *Pals1* CKO retinas. (**N**) The number of $CC3^+$ cells in *Pals1* CKO retinas at E17.5 and P0 (orange bars, $n = 6$) is ~8- and 3.5-fold increased compared with that of WT (green bars, $n = 3$). Scale bars, 48 μm.

previous finding in cortex deficient of *Pals1* (24). We also performed an in-depth analysis at E17.5 and P0 and observed ~8- and 3.5-fold increases in $CC3^+$ apoptotic cells in *Pals1* CKO retinas above those observed in the WT littermates [Fig. 7N, $n = 4$ ($P = 0.004132$) and $n = 3$ ($P = 0.00099$), respectively]. At adult stages, $CC3^+$ cells in *Pals1* CKO retinas were preferentially observed in the ONL where photoreceptor cells reside (Fig. 7O), showing a degeneration of photoreceptor cells in *Pals1*-deficient retinas. These results suggest that *Pals1*-deficient newly born retinal neurons at embryonic and postnatal stages and photoreceptor cells at later stages are vulnerable to apoptotic signal activation compared with the retinal progenitor cells.

Pals1 loss activates both astrocytes and microglia

Retinal damage caused by photoreceptor degeneration is often accompanied by characteristic changes in cell morphology and increased production of intermediate filament proteins in neighboring glial cells, including Muller glia, microglia and astrocytes, known as reactive gliosis (37).

To test whether *Pals1* deletion-mediated retinal damages could trigger reactive gliosis in Muller glia cells and/or retinal astrocytes, we assayed immuno-reactivity for glial fibrillary acidic protein (GFAP), an early marker of reactive gliosis in these cells (38). In P21 and P35 WT retinas, GFAP was exclusively detected in retinal astrocytes and in the end feet of Muller glia cells in the inner limiting membrane (Fig. 8A and C). GFAP immuno-reactivity began to increase and became greatly elevated in the radial processes and the inner limiting membrane in P21 and P35 *Pals1*-deficient retinas, respectively, suggesting the induction of reactive gliosis in *Pals1* CKO retinas (Fig. 8B and D). In addition, we observed some of the Muller processes extended above the OLM, reaching the subretinal space (see asterisks in Fig. 8B). We then examined microglia/macrophage activation, which mediates phagocytosis and the removal of cellular debris resulting from apoptotic cells predominantly in ganglion cell and inner nuclear layers (39,40). The number of retinal microglia/macrophages stained by Iba1 antibody, mainly localized in the inner and outer plexiform layers, and nerve fiber layer, was significantly increased and they were distributed throughout the entire retinal layers in P60 *Pals1* CKO retinas (Fig. 8E and F). These results are consistent with previous observations demonstrating microglia activation, proliferation and migration in other retinal degeneration mice (41,42).

DISCUSSION

Pals1 encodes a scaffolding protein essential for the assembly and function of the Crb polarity complex in epithelial tissues, including the retina. The Crb complex regulates cell polarity, cell shape and adhesion, cilia formation and cell proliferation (16,30,43,44). Abnormal regulation of the Crb complex is implicated in such disease processes as tumorigenesis, cystic kidney and retinal degeneration (13,20,21,31,45,46). The

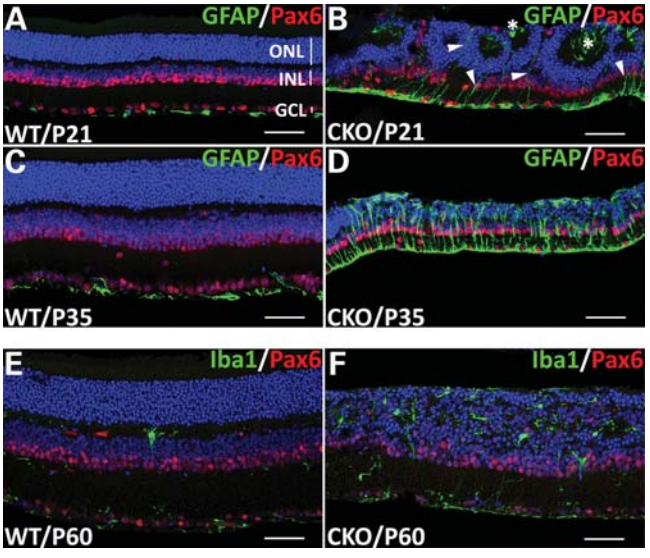

Figure 8. Upregulation of reactive gliosis markers in *Pals1* CKO retinas. GFAP immunostaining suggests the induction of reactive gliosis in *Pals1* CKO retinas. (**A**–**D**) Sections of P21 (A and B) and P35 (C and D) retinas from WT (A and C) and *Pals1* CKO (B and D) were stained with GFAP (green) to label retinal astrocytes in the inner limiting membrane and Pax6 in ganglion, amacrine and horizontal cells in ganglion cell and inner nuclear layers. (B and D) GFAP immuno-reactivity (green) starts to increase in Muller glia/astrocytes in *Pals1*-deficient retinas at P21 (arrowheads in B) and is highly upregulated at P35 (D). Apical processes of Muller glia cells are mislocalized in the subretinal space and the inner lumen of the pseudorosette (asterisks in B). (**E** and **F**) The section of P60 retinas stained with microglia/macrophage-specific Iba1 antibody shows the increased microglia/macrophage cells in the *Pals1*-deficient retinas (F) compared with that of WT control (E). Pax6 (red) staining shows the cells in inner nuclear and ganglion cell layer. Scale bars, 48 μm.

role of Crb polarity in the vertebrate retina has been extensively studied using *Crb1* mutant mice, which elucidated the vital adhesion function of the Crb complex at the OLM between photoreceptors and Muller glia cells (14,21,47). In this study, we disrupted the Crb polarity complex through genetic ablation of *Pals1* at the beginning of retinal development to address the function of Pals1 during embryonic and postnatal retinal development, and survival of the retinal neurons. The results presented here also provide the unique opportunity to visualize the cellular and molecular changes occurring in photoreceptor degeneration mediated by polarity defects.

Our studies with *Pals1* CKO mice have uncovered not only general defects that can be shared with other polarity gene mutations, but also novel phenotypes caused by disrupting the Crb polarity complex. The *Pals1* deletion partially disrupted the polarity of the retinas, which subsequently induced apical or basal displacement of retinal cells, as demonstrated by $pH3^+$, $Pax6^+$ and $Chx10^+$ cells (Fig. 6 and 7). Interestingly, we observed both apical and basal mislocation of the retinal cells, indicating the bi-directional disruption of the retinal polarity in *Pals1* CKO retinas. AJC defect-elicited laminar disorganization observed in the *Pals1* CKO retinas was initiated as early as E15.5. This disorganization is mediated by the disruption of the apical polarity complexes and adherens junction. Similar disturbances of embryonic retinal organization have been reported in genetic studies using the mutants of apical polarity genes, including PKC-λ, *nagie oko* (*nok*) (48,49), *oko meduzy* (*ome*) (30,50), and an adherens junction gene such as *glass onion* (*glo*) (51). For example, the PKC-λ mutant displays severe retinal lamination pattern defects due to defects in the junction between differentiating photoreceptors and retinal progenitors. In addition, the mutations of *nok* (zebra fish *Pals1* homolog), which normally localizes in the junctional complexes of retinal epithelium and photoreceptor cell layer, produce severe laminar defects, similar to *Pals1* CKO in our study. The *ome* mutations of the zebrafish Crb homolog, *crb2b*, display defects in the apical structure of the photoreceptors, leading to a disorganization of the entire retinal architecture. The *glo* (N-cadherin) zebrafish mutant exhibits retinal patterning defects by affecting the polarity of the neuroepithelia (52). Together, our results support that Pals1 plays a crucial role in retinal patterning by assembling functional apical polarity complex and maintaining the polarity and adhesion of the developing retinal epithelia.

We observed that an increased number of retinal postmitotic cells undergo caspase3-mediated cell death in the absence of Pals1. This induction of cell death causes retinal hypocellularity throughout the embryonic and postnatal stages. During embryonic development, the majority of dying cells were not retinal progenitor cells, but rather post-mitotic newly born retinal neurons including $Pax6^+$ amacrine/ganglion cells. Similarly, in the *Pals1*-deficient cortex, the apoptotic, precociously differentiated neurons were greatly increased at E12. However, the retinal cells showed a steady level of dying cells throughout the developmental and postnatal stages, whereas the *Pals1*-deficient cortex caused extensive apoptosis over a short period of time, peaking at E11 and E12. It was previously demonstrated that the extent of apoptotic cell death largely depends on the strength of the *Crb1* mutation. For example, $Crb1^{-/-}$ retinas showed degeneration of most retinal cell types except ganglion cells at the affected foci (47), whereas $Crb1^{C249W/-}$ retinas showed photoreceptor-specific cell death in the region (20). Interestingly *Pals1*-deficient retinas showed degeneration of most cell types at P14, as the retinal thinning and reduction of marker-specific cells were prominent in all three nuclear layers. Along with the embryonic manifestation of cell death, this observation suggests Pals1's general role in the survival of entire classes of retinal cells during embryonic and early postnatal stages. Pals1 is additionally required for the survival of retinal photoreceptor cells. At adult stages, the majority of dying cells are photoreceptor cells, indicating Pals1's specific role in the survival of photoreceptor cells in the mature retina.

Disrupted cell polarity is often associated with abnormal changes in cell proliferation behavior, including tumor development and progression (53,54). In cancers caused by viral oncogenes, the Crb polarity complex protein Patj degrades prior to malignant transformation (55,56). In *Pals1*-deficient mouse cortex, the size of the $BrdU^+$ progenitor pool was decreased due to defective progenitor self-renewal and elevated cell cycle exit (24). Although we found no statistically significant differences in cell proliferation between WT and *Pals1* CKO mice at E15.5 and E17.5 ($P > 0.005$), we did observe more variations in the fraction of $BrdU^+$ cells in the *Pals1* CKO retinas compared with those in the WT mice (25–39% in CKO compared with 29–34% in WT). This result may indicate that *Pals1* CKO retinas undergo a sudden increase and then subsequent decrease in cell

proliferation at or around E15.5. It is also likely that the observed transient increase in dividing cells in polarity defective retinas is compensated by a subsequent induction of cell death (Fig. 7). At E17.5, the size of the dividing retinal progenitor pool was decreased slightly, possibly due to a defect in maintaining retinal progenitors or to an increase of cell death in *Pals1* CKO retinas. This observation contrasts with previous work that reported a significantly decreased cortical progenitor pool in the developing *Pals1*-ablated cortex at E12 and E14 (24).

Pals1 is specifically required for full maturation of photoreceptor cells; premature formation of IS and/or OS in *Pals1* CKO retinas may facilitate degeneration. Generation of immature photoreceptor cells with shorter or deleted OS in several genetic mutants such as *Crx* and *Ahi1* is thought to undergo a similar degeneration pattern (1,2,32,57). In the *Crx* mutant, in which the OS formation is interrupted, photoreceptor cells degenerated, and ERG activity was lost at P30. In mutations of the *Ahi1*-encoded cilium-localizing protein, the opsin proteins were abnormally localized in the cytosol, and OS formation failed, both of which are analogous to *Pals1*-deficient photoreceptors. Since *Crx* and *Ahi1* encode transcription factors required for photoreceptor differentiation and protein localization to the cilium connecting IS and OS, respectively, it is intriguing to investigate the role of Pals1 in these processes.

Pals1 CKO mice exhibit the characteristics of human LCA patients, including the early loss of ERG and severe retinal degeneration. As determined by our ERG test, *Pals1* CKO mice showed visual impairment as early as P21, and we predict from the severely affected retinal tissues observed in our histologic analysis that the impairment may begin as early as P14 when the mice begin to open their eyes. Since we consistently observe critical features that distinguish LCA from RP, including lamination defects in early embryonic stages, early ERG loss and steady retinal degeneration, we propose our *Pals1* CKO mouse as a strong candidate for an LCA8-like model, recapitulating the pathologic features of human LCA8 patients caused by *Crb1* mutation. The absence of early-onset retinal dystrophy in any known mouse *Crb1* mutant may be explained by the functional compensation by related Crb2 or Crb3. It has been shown that *Dcx* (Doublecortin) mutant mice failed to reveal cortical neuronal migration defects exhibited in human patients, but the double-mutant with close homolog *Dclk* (Doublecortin-like kinase) successfully recapitulated the migration phenotypes (58,59). It is plausible that either double or triple KO of *Crb* family genes in mouse would induce the similar phenotypes that were observed in this study using *Pals1* CKO.

Interestingly, human LCA8 patients, regardless of age, exhibit coarsely laminated, thick central retina (the region around the fovea) (60–62), which is unlike other LCA patients with genetic mutations in RPE65 and GUCY2D, who show retinal thinning as a consequence of retinal degeneration. The *Pals1* CKO retinas in our study showed a temporally thick retina at E15.5, which then became thinner due to the increase of retinal cell death throughout developmental and adult stages. Nevertheless, both human LCA8 patients and *Pals1* CKO retinas share retinal lamination defects. Although it is difficult to understand the retinal thickening mechanism in human LCA8 patients with *CRB1* mutations, species differences may account for this dissimilarity, as rodents do not have a fovea. Consistent with this explanation, all mouse *Crb1* alleles tested also showed retinal thinning. The earliest stages that *Crb1* mutants exhibit the retinal phenotype varies from 4 weeks ($Crb1^{rd8}$) (21), to 3 months ($Crb1^{-/-}$) (47), to 8 months ($Crb1^{C249W}$) (20), which are all significantly later than the defects seen at E15.5 in the *Pals1* CKO mouse. In addition, *Pals1* CKO retinas show disruption/mislocalization of the interacting partners in the AJC of E15.5 retinas. The manifestation of this phenotype is significantly earlier than in the *Crb1* mutants, all of which show postnatal perturbations of the apically localizing proteins. Although the characteristics of postnatal defects exhibited in these *Crb1* mutants are similar to those of our *Pals1* CKO, the initiation and the extent of the retinal phenotypes are earlier and more severe in *Pals1* CKO mice. Recent studies utilizing a *Pals1* conditional knock-down (CKD) strategy has revealed the requirement for *Pals1* in the developing retina and RPE (63). *Pals1* CKD mice collectively exhibit similar but weaker and delayed defects, including partial disruption of apical proteins, laminar disorganization, persistent apoptotic activation and visual attenuation, compared with those of our *Pals1* CKO. Interestingly, RPE cells in *Pals1* CKD show altered structural features such as shortening of the apical villi, and increased size and number of vacuoles, thus suggesting the contribution of Pals1-mediated RPE phenotypes in LCA pathology. In our study, we observed relatively infrequent, disorganized RPE at E15.5 when *Pals1* was deleted with Rx-Cre (data not shown). This phenotype was not detected with Chx10-Cre, which is another retina-specific Cre line we used. This difference can be explained by critical differences in the two Cre lines we tested, including the extent, timing and heterogeneity of Cre expression in eye tissues. Since we observe a certain degree of laminar disorganization, although weak, in $Pals1^{f/f}$*;Chx10-Cre* mice (data not shown), we interpret that *Pals1* ablation in the retina plays a significant role in inducing LCA8-like phenotypes in $Pals1^{f/f}$*;Rx-Cre* mice, although the contribution of the RPE needs to be further characterized.

In the present study, we propose our *Pals1* CKO as an LCA8-like model mimicking the early-onset, and severe retinal degeneration of human patients. *Pals1* mutations have not been identified in human LCA patients, including LCA8, potentially due to the widespread expression of the gene in many tissues and its essential function during development. It is likely that human patients with *Pals1* mutations would display either lethality or syndromic LCA with multiple complications. Although Pals1 may not be responsible for any known or unknown LCA patients, our genetic studies have revealed the faithful recapitulation of many aspects of LCA phenotypes, highlighting the importance of the abnormal regulation of the Crb polarity complex in the pathogenesis of LCA. Furthermore, this study has uncovered the sequential changes in embryonic and postnatal phenotypes caused by *Pals1* ablation, revealing a time window for applying therapeutic interventions in pre-clinical settings of human LCA8. For example, retinal stem/progenitor cell- and gene-based therapies can be administered at neonatal stages during which photoreceptor cells remain relatively intact and the exogenous retinal environment promotes retinal differentiation.

MATERIALS AND METHODS

Animals, genotyping and generation of *Pals1* CKO mice

All animal handling, housing and experimentation were approved by and conducted under the guidelines of the University of Texas Health Animal Welfare Committee and the IACUC of the Baylor College of Medicine. *Pals1* flox allele and Rx-Cre line were described previously (24,26). The presence and absence of Rx-Cre was determined by PCR analysis, using two primers (sense: 5′GTTGGGAGAATGCTCCGT AA3′; antisense: 5′GTATCCCACAATTCCTTGCG3′). PCR genotyping was done as described previously (24). Animals with *Pals1* (*Pals1*$^{f/f}$) flox alleles were crossed with Rx-Cre transgenic mice (*Pals1*$^{f/+}$ */+;Rx-Cre*) to obtain the *Pals1* CKO (*Pals1*$^{f/f}$*;Rx-Cre/+*), heterozygote (*Pals1*$^{f/+}$*;Rx-Cre/+*) and WT control littermates (*Pals1*$^{f/+}$, *Pals1*$^{f/f}$, *Pals1*$^{+/+}$). The eyes/retinas from WT control littermates and/or age-matched BL6 mice were used as controls.

In situ hybridization, histology and immunofluorescence

Pals1 in situ hybridization was done as described previously (24). For histologic staining, we fixed the entire embryo heads and enucleated eyes of postnatal animals with 4% paraformaldehyde, embedded them in wax, sectioned and then stained them with hematoxylin and eosin (H&E), using standard methods. Retinal cells undergoing apoptosis were detected using α-CC3 antibody. For the immunofluorescence study, the histologic slides (either paraffin- or cryo-sectioned) were subjected to extensive antigen retrieval using citric acid (24), followed by incubation with a primary antibody overnight at 4°C. After three washes in PBS, the slides were incubated in a secondary antibody diluted 1:250 in blocking buffer [goat antibody to mouse conjugated with Cy3 and goat antibody to rabbit conjugated with Alexa488 (Jackson ImmunoResearch Laboratories, West Grove, PA, USA)] for 2 h at room temperature. Nuclear counterstaining was done with Hoechst33342 (1:1000, Invitrogen, Carlsbad, CA, USA) before mounting the cover slips with Fluore-G* slide-mounting medium (Southern Biotech, Inc., Birmingham, AL, USA). Visualization and imaging was achieved using an Axioplan 2 (Carl Zeiss Microimaging GmbH, Germany) or a confocal microscope (TCS SP5, Leica Microsystems GmbH, Wetzler, Germany).

Antibodies

Primary antibodies used in this study were: BrdU (mouse; 1:250, Sigma, St Louis, MO, USA), calbindin (mouse, 1:200, Abcam, Cambridge, MA, USA), N-cadherin and β-catenin (mouse, 1:200, BD Biosciences, Franklin Lakes, NJ, USA), CC3 (rabbit, 1:200, Cell Signaling Technology, Danvers, MA, USA), Chx10 (rabbit, 1:200, Abcam), cone arrestin (rabbit, 1:200, Dr Connie Cepko, Harvard Medical School, Boston, MA, USA), pan-Crb (rabbit, 1:300, Dr Jarema Malicki, Tufts Medical School, Boston, MA, USA), cyclin D1 (mouse, 1:200, Santa Cruz Biotechnology, Santa Cruz, CA, USA), Ezrin (mouse, 1:500, Abcam), GFAP (mouse, 1:400, Thermo Fisher Scientific, Fremont, CA, USA), GS (mouse, 1:300, BD Biosciences), Iba1 (rabbit, 1:200, Wako Pure Chemical Industries, Ltd, Richmond, VA, USA), pH3 (rabbit, 1:100, Millipore, Temecula, CA, USA), Pals1 (rabbit, 1:100, Millipore), Par3 (rabbit, 1:100, Millipore), Patj (rabbit, 1:300, Dr Andre le Bivic), Pax6 (mouse, 1:100, DSHB, Iowa City, IA, USA), Pax6 (rabbit, 1: 200, Covance, Emeryville, CA, USA), R4D2 [mouse, 1:200, (64)], β-tubulin III (mouse, 1:250, Covance).

Electron microscopy

For electron microscopy, the retinas were fixed in 3% glutaraldehyde, stored with Millonig's buffer for 5 min and replaced with 2% OsO_4 for 1 h at 4°C. Tissues were then washed with ddH_2O for 5 min and dehydrated by sequential standard ethanol wash, followed by propylene oxide, 50% LX-112, 100% LX-112 incubation. Tissues were embedded in a flat mold in a 70°C oven overnight for polymerization. Thick sections (500 nm) were cut using a Leica Ultracut-R microtome (Leica Microsystems GmbH) and a glass knife, heat-fixed to glass slides and stained with Toluidine Blue. 120 nm thin sections were cut using the same microtome and a diamond knife (Daitome, Hatfield, PA, USA), placed on a 150 mesh copper grid (EMS, Hatfield, PA, USA) and stained for 15 min with 2% uranyl acetate, rinsed with ddH_2O, stained for 5 min in Reynold's lead citrate, rinsed and dried in a 70°C oven. Images were obtained from the JOEL 1200 Transmission Electron Microscope at 60 kV and captured with the 1 k × 1 k Gatan Digital Imaging System (Electron Microscopy Laboratory, Department of Pathology, UTHSC, Houston, TX, USA).

Electroretinography

ERG was performed as described previously (65). Briefly, animals were dark-adapted for at least 10 h before being subjected to ERG testing. Dark-adapted mice were anesthetized with an intramuscular injection of ketamine (37.6 mg/ml), xylazine (1.92 mg/ml) and acepromazine (0.38 mg/ml). Pupils were dilated with 1% tropicamide and 2.5% phenylephrine, and 0.5% proparacaine was applied for corneal anesthesia. The voltage difference between the corneal and reference electrodes is amplified by a Grass P122 amplifier, and the amplified signal was digitized by a National Instruments (BNC-2090) board, and the digital waveforms were stored by a custom Matlab program.

X-gal staining

Retinal sections of WT and/or *Pals1* CKO were post-fixed with 4% paraformaldehyde in PBS on ice for 30 min, rinsed three times in PBS and stained in X-gal reaction buffer containing 35 mM potassium ferrocyanide, 35 mM potassium ferricyanide, 2 mM $MgCl_2$, 0.02% Nonidet P-40, 0.01% sodium deoxycholate and X-gal for 1 to several hours at 37°C.

Quantification of S- and M-phase retinal progenitor cells

Pregnant females harboring E15.5 and E17.5 embryos were intraperitoneally injected with BrdU (50 mg/kg body weight) 30 min before tissue harvest. Seven micrometers of paraffin

sections were stained for BrdU (Harlan Laboratories) and phosphor-histone H3 (pH3). Quantification was conducted on more than three retinas from both WT and *Pals1* CKO mice. Hoechst33258$^+$ and BrdU$^+$ or pH3$^+$ cells were manually counted using Photoshop and ImageJ v1.38x (W. Rasband, National Institute of Health, Bethesda, MD, USA) from confocal images obtained in *Pasl1* CKO and WT (Leica TCS SP5, Leica Microsystems).

Quantification of apoptotic cells

Apoptotic cells were stained with α-CC3 antibody at E15.5, E17.5, P0 and P35. More than three retinas showing lamination defects at E17.5 and P0 *Pals1* CKO and six control WT retinal counterparts were used for quantification. Total dying cell numbers were determined by manual counting of CC3$^+$ cells per frame using Photoshop and ImageJ v1.38x (W. Rasband) in *Pals1* CKO and WT retinal images obtained from confocal microscope (Leica TCS SP5, Leica Microsystems).

ACKNOWLEDGEMENTS

We thank Dr Michael Gambello (University of Texas Health Science Center at Houston) for the valuable suggestions and discussion on this manuscript. We are indebted to Dr Cepko for providing Chx10-Cre mouse and cone arrestin antibody. We also thank Drs le Bivic and Malicki for providing Patj and pan-Crb antibodies, respectively. For mouse α-Pax6 antibody, the monoclonal antibody developed by Dr Atsushi Kawakami (Tokyo Institute of Technology, Japan) was obtained from the Developmental Studies Hybridoma Bank developed under the auspices of the NICHD and maintained by The University of Iowa, Department of Biology, Iowa City, IA 52242, USA. Additionally, we thank Ms Patricia Navarro and Mr Steven Kolodziej in the Department of Pathology and Laboratory of Medicine, University of Texas Health Science Center at Houston for the help in preparing electron microscope samples.

Conflict of Interest statement. None declared.

FUNDING

This work was supported by the NIH grants to S.-H.C. (R01EY020578) and S.K. (R01NS073112).

REFERENCES

1. Westfall, J.E., Hoyt, C., Liu, Q., Hsiao, Y.C., Pierce, E.A., Page-McCaw, P.S. and Ferland, R.J. (2010) Retinal degeneration and failure of photoreceptor outer segment formation in mice with targeted deletion of the Joubert syndrome gene, Ahi1. *J. Neurosci.*, **30**, 8759–8768.
2. Furukawa, T., Morrow, E.M., Li, T., Davis, F.C. and Cepko, C.L. (1999) Retinopathy and attenuated circadian entrainment in Crx-deficient mice. *Nat. Genet.*, **23**, 466–470.
3. Omri, S., Omri, B., Savoldelli, M., Jonet, L., Thillaye-Goldenberg, B., Thuret, G., Gain, P., Jeanny, J.C., Crisanti, P. and Behar-Cohen, F. (2010) The outer limiting membrane (OLM) revisited: clinical implications. *Clin. Ophthalmol.*, **4**, 183–195.
4. den Hollander, A.I., Roepman, R., Koenekoop, R.K. and Cremers, F.P. (2008) Leber congenital amaurosis: genes, proteins and disease mechanisms. *Prog. Retin. Eye Res.*, **27**, 391–419.
5. den Hollander, A.I., ten Brink, J.B., de Kok, Y.J., van Soest, S., van den Born, L.I., van Driel, M.A., van de Pol, D.J., Payne, A.M., Bhattacharya, S.S., Kellner, U. *et al.* (1999) Mutations in a human homologue of *Drosophila* crumbs cause retinitis pigmentosa (RP12). *Nat. Genet.*, **23**, 217–221.
6. Pellikka, M., Tanentzapf, G., Pinto, M., Smith, C., McGlade, C.J., Ready, D.F. and Tepass, U. (2002) Crumbs, the *Drosophila* homologue of human CRB1/RP12, is essential for photoreceptor morphogenesis. *Nature*, **416**, 143–149.
7. Lotery, A.J., Jacobson, S.G., Fishman, G.A., Weleber, R.G., Fulton, A.B., Namperumalsamy, P., Heon, E., Levin, A.V., Grover, S., Rosenow, J.R. *et al.* (2001) Mutations in the CRB1 gene cause Leber congenital amaurosis. *Arch. Ophthalmol.*, **119**, 415–420.
8. Richard, M., Roepman, R., Aartsen, W.M., van Rossum, A.G., den Hollander, A.I., Knust, E., Wijnholds, J. and Cremers, F.P. (2006) Towards understanding CRUMBS function in retinal dystrophies. *Hum. Mol. Genet.,* **15** (Spec no. 2), R235–R243.
9. Kamberov, E., Makarova, O., Roh, M., Liu, A., Karnak, D., Straight, S. and Margolis, B. (2000) Molecular cloning and characterization of Pals, proteins associated with mLin-7. *J. Biol. Chem.*, **275**, 11425–11431.
10. Roh, M.H., Makarova, O., Liu, C.J., Shin, K., Lee, S., Laurinec, S., Goyal, M., Wiggins, R. and Margolis, B. (2002) The Maguk protein, Pals1, functions as an adapter, linking mammalian homologues of Crumbs and Discs Lost. *J. Cell Biol.*, **157**, 161–172.
11. Michel, D., Arsanto, J.P., Massey-Harroche, D., Beclin, C., Wijnholds, J. and Le Bivic, A. (2005) PATJ connects and stabilizes apical and lateral components of tight junctions in human intestinal cells. *J. Cell Sci.*, **118**, 4049–4057.
12. Gosens, I., den Hollander, A.I., Cremers, F.P. and Roepman, R. (2008) Composition and function of the Crumbs protein complex in the mammalian retina. *Exp. Eye Res.*, **86**, 713–726.
13. Bulgakova, N.A. and Knust, E. (2009) The Crumbs complex: from epithelial-cell polarity to retinal degeneration. *J. Cell Sci.*, **122**, 2587–2596.
14. van Rossum, A.G., Aartsen, W.M., Meuleman, J., Klooster, J., Malysheva, A., Versteeg, I., Arsanto, J.P., Le Bivic, A. and Wijnholds, J. (2006) Pals1/Mpp5 is required for correct localization of Crb1 at the subapical region in polarized Muller glia cells. *Hum. Mol. Genet.*, **15**, 2659–2672.
15. Bazellieres, E., Assemat, E., Arsanto, J.P., Le Bivic, A. and Massey-Harroche, D. (2009) Crumbs proteins in epithelial morphogenesis. *Front. Biosci.*, **14**, 2149–2169.
16. Wang, Q. and Margolis, B. (2007) Apical junctional complexes and cell polarity. *Kidney Int.*, **72**, 1448–1458.
17. Wang, Q., Hurd, T.W. and Margolis, B. (2004) Tight junction protein Par6 interacts with an evolutionarily conserved region in the amino terminus of PALS1/stardust. *J. Biol. Chem.*, **279**, 30715–30721.
18. Hurd, T.W., Gao, L., Roh, M.H., Macara, I.G. and Margolis, B. (2003) Direct interaction of two polarity complexes implicated in epithelial tight junction assembly. *Nat. Cell Biol.*, **5**, 137–142.
19. Assemat, E., Bazellieres, E., Pallesi-Pocachard, E., Le Bivic, A. and Massey-Harroche, D. (2008) Polarity complex proteins. *Biochim. Biophys. Acta*, **1778**, 614–630.
20. van de Pavert, S.A., Meuleman, J., Malysheva, A., Aartsen, W.M., Versteeg, I., Tonagel, F., Kamphuis, W., McCabe, C.J., Seeliger, M.W. and Wijnholds, J. (2007) A single amino acid substitution (Cys249Trp) in Crb1 causes retinal degeneration and deregulates expression of pituitary tumor transforming gene Pttg1. *J. Neurosci.*, **27**, 564–573.
21. Mehalow, A.K., Kameya, S., Smith, R.S., Hawes, N.L., Denegre, J.M., Young, J.A., Bechtold, L., Haider, N.B., Tepass, U., Heckenlively, J.R. *et al.* (2003) CRB1 is essential for external limiting membrane integrity and photoreceptor morphogenesis in the mammalian retina. *Hum. Mol. Genet.*, **12**, 2179–2189.
22. van den Hurk, J.A., Rashbass, P., Roepman, R., Davis, J., Voesenek, K.E., Arends, M.L., Zonneveld, M.N., van Roekel, M.H., Cameron, K., Rohrschneider, K. *et al.* (2005) Characterization of the Crumbs homolog 2 (CRB2) gene and analysis of its role in retinitis pigmentosa and Leber congenital amaurosis. *Mol. Vis.*, **11**, 263–273.
23. Straight, S.W., Shin, K., Fogg, V.C., Fan, S., Liu, C.J., Roh, M. and Margolis, B. (2004) Loss of PALS1 expression leads to tight junction and polarity defects. *Mol. Biol. Cell*, **15**, 1981–1990.
24. Kim, S., Lehtinen, M.K., Sessa, A., Zappaterra, M.W., Cho, S.H., Gonzalez, D., Boggan, B., Austin, C.A., Wijnholds, J., Gambello, M.J.

et al. (2010) The apical complex couples cell fate and cell survival to cerebral cortical development. *Neuron*, **66**, 69–84.
25. den Hollander, A.I., Ghiani, M., de Kok, Y.J., Wijnholds, J., Ballabio, A., Cremers, F.P. and Broccoli, V. (2002) Isolation of Crb1, a mouse homologue of *Drosophila* crumbs, and analysis of its expression pattern in eye and brain. *Mech. Dev.*, **110**, 203–207.
26. Swindell, E.C., Bailey, T.J., Loosli, F., Liu, C., Amaya-Manzanares, F., Mahon, K.A., Wittbrodt, J. and Jamrich, M. (2006) Rx-Cre, a tool for inactivation of gene expression in the developing retina. *Genesis*, **44**, 361–363.
27. Rowan, S. and Cepko, C.L. (2004) Genetic analysis of the homeodomain transcription factor Chx10 in the retina using a novel multifunctional BAC transgenic mouse reporter. *Dev. Biol.*, **271**, 388–402.
28. Koike, C., Nishida, A., Akimoto, K., Nakaya, M.A., Noda, T., Ohno, S. and Furukawa, T. (2005) Function of atypical protein kinase C lambda in differentiating photoreceptors is required for proper lamination of mouse retina. *J. Neurosci.*, **25**, 10290–10298.
29. Wei, X. and Malicki, J. (2002) nagie oko, encoding a MAGUK-family protein, is essential for cellular patterning of the retina. *Nat. Genet.*, **31**, 150–157.
30. Omori, Y. and Malicki, J. (2006) oko meduzy and related crumbs genes are determinants of apical cell features in the vertebrate embryo. *Curr. Biol.*, **16**, 945–957.
31. van de Pavert, S.A., Kantardzhieva, A., Malysheva, A., Meuleman, J., Versteeg, I., Levelt, C., Klooster, J., Geiger, S., Seeliger, M.W., Rashbass, P. *et al.* (2004) Crumbs homologue 1 is required for maintenance of photoreceptor cell polarization and adhesion during light exposure. *J. Cell Sci.*, **117**, 4169–4177.
32. Louie, C.M., Caridi, G., Lopes, V.S., Brancati, F., Kispert, A., Lancaster, M.A., Schlossman, A.M., Otto, E.A., Leitges, M., Grone, H.J. *et al.* (2010) AHI1 is required for photoreceptor outer segment development and is a modifier for retinal degeneration in nephronophthisis. *Nat. Genet.*, **42**, 175–180.
33. Gao, J., Cheon, K., Nusinowitz, S., Liu, Q., Bei, D., Atkins, K., Azimi, A., Daiger, S.P., Farber, D.B., Heckenlively, J.R. *et al.* (2002) Progressive photoreceptor degeneration, outer segment dysplasia, and rhodopsin mislocalization in mice with targeted disruption of the retinitis pigmentosa-1 (Rp1) gene. *Proc. Natl Acad. Sci. USA*, **99**, 5698–5703.
34. Medina, E., Williams, J., Klipfell, E., Zarnescu, D., Thomas, G. and Le Bivic, A. (2002) Crumbs interacts with moesin and beta(Heavy)-spectrin in the apical membrane skeleton of *Drosophila*. *J. Cell Biol.*, **158**, 941–951.
35. Wodarz, A. (2005) Molecular control of cell polarity and asymmetric cell division in *Drosophila* neuroblasts. *Curr. Opin. Cell Biol.*, **17**, 475–481.
36. Ceron, J., Gonzalez, C. and Tejedor, F.J. (2001) Patterns of cell division and expression of asymmetric cell fate determinants in postembryonic neuroblast lineages of *Drosophila*. *Dev. Biol.*, **230**, 125–138.
37. Wohl, S.G., Schmeer, C.W., Friese, T., Witte, O.W. and Isenmann, S. (2011) In situ dividing and phagocytosing retinal microglia express nestin, vimentin, and NG2 in vivo. *PLoS One*, **6**, e22408.
38. Chen, H. and Weber, A.J. (2002) Expression of glial fibrillary acidic protein and glutamine synthetase by Muller cells after optic nerve damage and intravitreal application of brain-derived neurotrophic factor. *Glia*, **38**, 115–125.
39. Langmann, T. (2007) Microglia activation in retinal degeneration. *J. Leukoc. Biol.*, **81**, 1345–1351.
40. Imai, Y. and Kohsaka, S. (2002) Intracellular signaling in M-CSF-induced microglia activation: role of Iba1. *Glia*, **40**, 164–174.
41. Zeiss, C.J. and Johnson, E.A. (2004) Proliferation of microglia, but not photoreceptors, in the outer nuclear layer of the rd-1 mouse. *Invest. Ophthalmol. Vis. Sci.*, **45**, 971–976.
42. Zeng, H.Y., Zhu, X.A., Zhang, C., Yang, L.P., Wu, L.M. and Tso, M.O. (2005) Identification of sequential events and factors associated with microglial activation, migration, and cytotoxicity in retinal degeneration in rd mice. *Invest. Ophthalmol. Vis. Sci.*, **46**, 2992–2999.
43. Fan, S., Hurd, T.W., Liu, C.J., Straight, S.W., Weimbs, T., Hurd, E.A., Domino, S.E. and Margolis, B. (2004) Polarity proteins control ciliogenesis via kinesin motor interactions. *Curr. Biol.*, **14**, 1451–1461.
44. Richardson, E.C. and Pichaud, F. (2010) Crumbs is required to achieve proper organ size control during *Drosophila* head development. *Development*, **137**, 641–650.
45. Karp, C.M., Tan, T.T., Mathew, R., Nelson, D., Mukherjee, C., Degenhardt, K., Karantza-Wadsworth, V. and White, E. (2008) Role of the polarity determinant crumbs in suppressing mammalian epithelial tumor progression. *Cancer Res.*, **68**, 4105–4115.
46. Olsen, O., Funke, L., Long, J.F., Fukata, M., Kazuta, T., Trinidad, J.C., Moore, K.A., Misawa, H., Welling, P.A., Burlingame, A.L. *et al.* (2007) Renal defects associated with improper polarization of the CRB and DLG polarity complexes in MALS-3 knockout mice. *J. Cell Biol.*, **179**, 151–164.
47. van de Pavert, S.A., Sanz, A.S., Aartsen, W.M., Vos, R.M., Versteeg, I., Beck, S.C., Klooster, J., Seeliger, M.W. and Wijnholds, J. (2007) Crb1 is a determinant of retinal apical Muller glia cell features. *Glia*, **55**, 1486–1497.
48. Wei, X., Zou, J., Takechi, M., Kawamura, S. and Li, L. (2006) Nok plays an essential role in maintaining the integrity of the outer nuclear layer in the zebrafish retina. *Exp. Eye Res.*, **83**, 31–44.
49. Zou, J., Lathrop, K.L., Sun, M. and Wei, X. (2008) Intact retinal pigment epithelium maintained by Nok is essential for retinal epithelial polarity and cellular patterning in zebrafish. *J. Neurosci.*, **28**, 13684–13695.
50. Malicki, J. and Driever, W. (1999) oko meduzy mutations affect neuronal patterning in the zebrafish retina and reveal cell-cell interactions of the retinal neuroepithelial sheet. *Development*, **126**, 1235–1246.
51. Pujic, Z. and Malicki, J. (2001) Mutation of the zebrafish glass onion locus causes early cell-nonautonomous loss of neuroepithelial integrity followed by severe neuronal patterning defects in the retina. *Dev. Biol.*, **234**, 454–469.
52. Malicki, J., Jo, H. and Pujic, Z. (2003) Zebrafish N-cadherin, encoded by the glass onion locus, plays an essential role in retinal patterning. *Dev. Biol.*, **259**, 95–108.
53. Wodarz, A., Grawe, F. and Knust, E. (1993) CRUMBS is involved in the control of apical protein targeting during *Drosophila* epithelial development. *Mech. Dev.*, **44**, 175–187.
54. Igaki, T., Pagliarini, R.A. and Xu, T. (2006) Loss of cell polarity drives tumor growth and invasion through JNK activation in *Drosophila*. *Curr. Biol.*, **16**, 1139–1146.
55. Javier, R.T. (2008) Cell polarity proteins: common targets for tumorigenic human viruses. *Oncogene*, **27**, 7031–7046.
56. Storrs, C.H. and Silverstein, S.J. (2007) PATJ, a tight junction-associated PDZ protein, is a novel degradation target of high-risk human papillomavirus E6 and the alternatively spliced isoform 18 E6. *J. Virol.*, **81**, 4080–4090.
57. Pignatelli, V., Cepko, C.L. and Strettoi, E. (2004) Inner retinal abnormalities in a mouse model of Leber's congenital amaurosis. *J. Comp. Neurol.*, **469**, 351–359.
58. Deuel, T.A., Liu, J.S., Corbo, J.C., Yoo, S.Y., Rorke-Adams, L.B. and Walsh, C.A. (2006) Genetic interactions between doublecortin and doublecortin-like kinase in neuronal migration and axon outgrowth. *Neuron*, **49**, 41–53.
59. Koizumi, H., Tanaka, T. and Gleeson, J.G. (2006) Doublecortin-like kinase functions with doublecortin to mediate fiber tract decussation and neuronal migration. *Neuron*, **49**, 55–66.
60. Jacobson, S.G., Cideciyan, A.V., Aleman, T.S., Pianta, M.J., Sumaroka, A., Schwartz, S.B., Smilko, E.E., Milam, A.H., Sheffield, V.C. and Stone, E.M. (2003) Crumbs homolog 1 (CRB1) mutations result in a thick human retina with abnormal lamination. *Hum. Mol. Genet.*, **12**, 1073–1078.
61. Aleman, T.S., Cideciyan, A.V., Aguirre, G.K., Huang, W.C., Mullins, C.L., Roman, A.J., Sumaroka, A., Olivares, M.B., Tsai, F.F., Schwartz, S.B. *et al.* (2011) Human CRB1-associated retinal degeneration: comparison with the rd8 Crb1-mutant mouse model. *Invest. Ophthalmol. Vis. Sci.*, **52**, 6898–6910.
62. Henderson, R.H., Mackay, D.S., Li, Z., Moradi, P., Sergouniotis, P., Russell-Eggitt, I., Thompson, D.A., Robson, A.G., Holder, G.E., Webster, A.R. *et al.* (2011) Phenotypic variability in patients with retinal dystrophies due to mutations in CRB1. *Br. J. Ophthalmol.*, **95**, 811–817.
63. Park, B., Alves, C.H., Lundvig, D.M., Tanimoto, N., Beck, S.C., Huber, G., Richard, F., Klooster, J., Andlauer, T.F., Swindell, E.C. *et al.* (2011) PALS1 is essential for retinal pigment epithelium structure and neural retina stratification. *J. Neurosci.*, **31**, 17230–17241.
64. Molday, R.S. and MacKenzie, D. (1983) Monoclonal antibodies to rhodopsin: characterization, cross-reactivity, and application as structural probes. *Biochemistry*, **22**, 653–660.
65. Abd-El-Barr, M.M., Pennesi, M.E., Saszik, S.M., Barrow, A.J., Lem, J., Bramblett, D.E., Paul, D.L., Frishman, L.J. and Wu, S.M. (2009) Genetic dissection of rod and cone pathways in the dark-adapted mouse retina. *J. Neurophysiol.*, **102**, 1945–1955.